

Design of Hybrid Solid Polymer Electrolytes: Structure and Properties

Lyudmila M. Bronstein,^{1} Robert L. Karlinsey,¹ Kyle Ritter,^{1§} Chan Gyu Joo,¹ Barry Stein,² and Josef*

W. Zwanziger^{1ψ}

Departments of Chemistry¹ and Biology², Indiana University, Bloomington, IN 47405

RECEIVED DATE (to be automatically inserted after your manuscript is accepted if required according to the journal that you are submitting your paper to)

ABSTRACT. This paper reports synthesis, structure, and properties of novel hybrid solid polymer electrolytes (SPEs) consisting of organically modified aluminosilica (OM-AISi), formed within a

*To whom correspondence should be addressed (lybronst@indiana.edu)

§ Current address for KR: Depts. of Materials Science and Engineering, University of Illinois 405 North Mathews Avenue, Urbana, IL 61801.

ψ Current address for JWZ: Dept. of Chemistry, Dalhousie University, Halifax, NS, B3H 4J3 Canada.

poly(ethylene oxide)-in-salt (Li triflate) phase. To alter the structure and properties of these polymer electrolytes, we used functionalized silanes containing poly(ethylene oxide) (PEO) tails or CN groups. The SPEs described here were studied using differential scanning calorimetry, Raman spectroscopy, X-ray powder diffraction, and AC impedance spectroscopy. The size of the OM-AISi domains was estimated using transmission electron microscopy and comparing the sizes of AISi nanoparticles, obtained via calcination of the hybrid SPE. The conductivity enhancement, caused by incorporation of PEO tails or CN groups in the hybrid materials based on 600 Da poly(ethylene glycol), can be ascribed to a decrease of OM-AISi domain size accompanied with an increase of the OM-AISi/PEO+LiTf interface. For the CN modifier, increase of this interface increases the amount of CN groups exposed to PEO+LiTf phase, thus increasing the effective dielectric constants of the materials and their conductivity, although this dependence is not linear. In the case of the PEO modifier, different effects are observed for 600 Da PEG and 100 KDa PEO. For 100 KDa PEO, incorporation of the silane with a PEO tail caused a decrease of conductivity. Here, AISi particle size remains basically unchanged with addition of silane-modifier, and the decrease of conductivity can be attributed to formation of a crystalline phase at the OM-AISi/PEO+LiTf interface.

Introduction

Recently, hybrid organic-inorganic solid polymer electrolytes (SPEs) consisting of a conventional salt-in-polymer electrolyte together with an inorganic component have drawn the attention of several research groups. These materials display a number of advantages compared to simple salt-in-polymer electrolytes and are believed to be promising materials for application in secondary lithium batteries.¹⁻¹⁴ Advantages include the suppression of PEO crystallization and the enhancement of the mechanical properties. In many cases, composite electrolytes also show higher conductivity and Li transference numbers, which are crucial for successful application in Li batteries. Among the inorganic components incorporated in composite polymer electrolytes, the most popular are inorganic fillers (Al_2O_3 , SiO_2 , TiO_2 etc.), with particle sizes varying from microns to nanometers.^{2,9-11,15-18} Several papers have

reported that the decrease of filler size to the nanometer scale, which leads to significant increase of interfacial surface area, yields improved solid polymer electrolyte properties.^{19,20} In a different approach, composite materials based on clay platelets (intercalate materials) displayed strongly modified properties with a very weak temperature dependence of conductivity.²¹ These polymer-inorganic intercalate materials may however display anisotropy in their properties.²²⁻²⁴ Recently, it was demonstrated that the improvement of polymer electrolyte conductivity, when nanoparticles are introduced, is mainly due to suppression of crystallization of the 'PEO+Li salt' phase, while for fully amorphous PEO no effect was found (i.e., no ion aggregation suppression was observed).^{25,26} In contrast, it has also been reported that positive effects of the filler incorporation are observed also for fully amorphous polymers.¹⁰ In our opinion, a more favorable option for development of composite materials with inorganic component is realized when the latter forms *in situ* within the polymer matrix, as demonstrated in ref.^{27,28} *In situ* formation results in a "fresh" surface of inorganic component, while preformed fillers may have already-modified surfaces (especially nanoparticles, which are normally stabilized during preparation). In the case of *in situ* formation of the inorganic component, both nanoparticles and interpenetrating networks can be obtained, depending on the reaction conditions and the ratio of organic and inorganic components. In some cases, organic and inorganic components can be merely intimately mixed,²⁹ while in others, they can be chemically bonded.^{27,28,30}

Earlier we reported on the structure and properties of SPEs built from two major components: organically modified aluminosilicate (denoted here as OM-ALSi) prepared by hydrolytic condensation of (3-glycidoxypropyl)trimethoxysilane (GLYMO) and Al(tri-*sec*-butoxide), and a conventional salt-in-polymer constituent.^{28,31,32} Here, poly(ethylene oxide) (PEO) is used as polymer and Li triflate (LiTf) as Li salt. The pure OM-ALSi based on GLYMO and aluminum tri-*sec*-butoxide was described in ref.³³. As shown in Scheme 1, hydrolysis of GLYMO and aluminum tri-*sec*-butoxide, followed by condensation and polymerization in the salt-in-polymer medium, leads to aluminosilica containing different Si and Al sites intimately mixed with the polymer. As OM-ALSi is condensed within the salt-in-polymer component, fresh OM-ALSi/PEO+LiTf interface is developed. The glycidyl group of GLYMO,

ensuring compatibility with PEO, is polymerized in the presence of Al(tri-*sec*-butoxide), which leads to additional crosslinking within OM-AlSi. The overall structure of the OM-AlSi-based SPE depends on the OM-AlSi loading as well as other parameters.²⁸ These hybrid SPEs show improved properties over salt-in-polymer electrolytes, but still there is room for additional improvement: the conductivities of these SPE are quite far from the high conductivity values of liquid electrolytes. The multicomponent nature of this system, which contains OM-AlSi (in turn, based on two precursors), PEO, and Li triflate, allows an excellent opportunity to enhance and to tailor the properties of these SPE by chemical modification of either OM-AlSi or a polymeric part. There are two obvious routes to follow. First, one may attempt to lower the glass transition temperature, so that mobility at ambient temperature is improved. Secondly, one may try to increase the dielectric constant of the material, so that ion aggregation is suppressed. In this paper we report on results of both these approaches.

Experimental Methods

Materials

Poly(ethylene glycol) (PEG) and poly(ethylene oxide) (PEO) with molecular weights of 600 and 100,000, respectively, were purchased from Aldrich and used as received. Li triflate, THF, aluminum tri-*sec*-butoxide (Aldrich), chloroform (EM Ind., Inc.), (3-glycidylpropyl)trimethoxysilane (GLYMO, Fluka) were used without further purification. [Methoxy(polyethylenoxy)propyl]trimethoxysilane (MPEOP) and 2-cyanoethyltrimethoxysilane (CN) were purchased from Gelest and used as received. Water was purified with a “Barnstead NANOpure water” purification system.

Synthesis

Synthesis of non-modified organic-inorganic composite based on PEO (OM-AlSi-PEO) was carried out as described elsewhere.²⁸ In a typical experiment, 0.4 g (9 mmol) PEO in 5 ml chloroform were mixed with 0.1 g (0.64 mmol) Li triflate in 5 ml THF. After 30 min stirring, the solution was kept aside. The inorganic part of the hybrid was prepared by hydrolysis of the mixture of GLYMO with Al tri-*sec*-butoxide in molar ratio 80:20, respectively. Hydrolysis was initiated by addition of 15% of equimolar amount of water containing HCl (0.01 N solution). After 15 min stirring at ~0 °C (water-ice bath) and

15 min at room temperature, the reaction mixture was charged with the residue of the 0.01 N HCl solution and stirred for 20 min. The prehydrolyzed sol was added to the solution containing PEO and Li salt (amount was determined by the desired ratio of PEO:inorganic hybrid, which varied in the range of 40-70 wt.%) and stirred for 1 h. Afterwards the solvents were evaporated on a Teflon dish at 65-70 °C for 2 h. The solid film was treated at 130 °C in vacuum for 1 h to complete condensation. Films were easily removed from the dish and ready for examination. Samples were sealed and kept in dessicator. As shown in ref. ²⁸, weight loss from apparent water (up to 150 °C) did not exceed 0.5%. In the modified samples, certain fraction of GLYMO was replaced with the same mole amount of a corresponding modifier (MPEOP or CN) added to OM-AISi mixture together with GLYMO.

Characterization

Raman spectra were acquired on a Renishaw RM2000 Raman Microscope using a 785 nm diode laser for excitation. The Raman spectra were averaged from several scans. A total acquisition time from 30 min to 1h was used.

Samples for transmission electron microscopy (TEM) were prepared by grinding the calcined samples using a mortar and pestle followed by suspension in acetone. A drop of the sample suspension was placed onto a carbon-coated copper grid. The acetone was then evaporated off at room temperature. Images were acquired at accelerating voltage of 60 kV on JEOL JEM1010 microscope.

Differential scanning calorimetry (DSC) was performed with a Perkin-Elmer DSC 7 calorimeter. Sample masses varied from 5-20 mg and were hermetically sealed in aluminum pans. Samples were scanned between -100°C and +100°C at a rate of 10°C/min, using liquid nitrogen as the coolant. Glass transition regions were then determined using the fictive temperature method in the Pyris software. Both indium and cyclohexane were used to reference thermal events. Melting points and associated enthalpies were analyzed by deconvolution since observed endothermic transitions were not symmetric. Up to four Gaussians were used to accurately capture the character of the transition. The melting points reflect the center of gravity melting, and the tabulated enthalpy is the sum of the peak-fit areas.

AC impedance spectroscopy was used to measure conductivity and dielectric constants of cast films. To obtain excellent electrode-electrolyte contact, gold electrodes of a known area (0.0647 cm^2) were directly attached to the film by sputter coating, using a Polaron E5100 Sputter Coater. Films were then placed in a home-built temperature controlled cell for measurements. Room and variable temperature measurements were performed with a HP 4192A Impedance Analyzer, and a Quantum Design Digital RG Bridge Model 1802 was used to vary and monitor the cell temperature. The admittance response of the material was collected by sweeping the frequencies from 5 Hz to 13 MHz with a 1 V signal, using the standard circuit model of a resistor and capacitor in parallel. Bulk resistances were then extrapolated by fitting a linear regression to the bulk response of the material. Both silicon and $(\text{PEO})_{14}\text{LiTf}$ were used as reference materials for conductivity. Dielectric constants were obtained by taking the minimum in a capacitance versus frequency curve. Pure PEO ($\epsilon_r \sim 5$)³⁴ was used as a reference material.

Powder diffraction patterns were collected on a Scintag theta-theta powder diffractometer. X-rays were generated from a copper target with a scattering wavelength of 1.54 \AA . The step-size of the experiment was 0.03° . We used Cerius² software to simulate the powder pattern based on single-crystal PEO data³⁵ in order to index the Bragg peaks of the experimental powder pattern. Indexing to a monoclinic cell³⁵ revealed one prominent peak with separation 4.64 \AA , corresponding to d_{120} , while the other feature at 3.82 \AA matched closely with d_{032} but revealed some overlap of adjacent reflections as observed in the simulated powder pattern. Due to this interference at 3.82 \AA , however, our discussion only emphasizes d_{120} modulations. The data was then converted to q -space and deconvoluted by fitting a single Gaussian to the d_{120} Bragg reflection. This deconvolution allowed an estimate of the peak center of gravity, FWHM, and crystal size.

Solid-state ^{27}Al MAS NMR was performed using a Bruker Avance DSX spectrometer. Spectra from both nuclei were obtained using a 4mm Magic Angle Spinning (MAS) probe with the spin rate locked at 10 kHz. A single, short pulse of length 0.5 \mu sec with a recycle time of 0.15 seconds was used to acquire ^{27}Al spectra. All spectra were referenced to corundum.

Results and Discussion

1. Modification of OM-AISi

The conductivity and transference number of an SPE are determined by a number of factors, including Li ion mobility and the number density of free lithium ions. By influencing these factors, one may enhance the conductivity and improve other important SPE characteristics. As is well established, lowering the glass transition temperature by adding plasticizers is one route to enhancing conductivity.⁹
¹⁰ Another possible avenue in achieving higher conductivity is addition of a modifier with a high dielectric constant. Presumably, increase of dielectric constant should increase the degree of dissociation of a lithium salt, thus increasing conductivity and transference number. However, if the plasticizer or dielectric constant modifier is a small molecule, it can leach, changing the polymer electrolyte properties with the passage of time. Alternatively, if a modifier is covalently attached to the immobile components of SPE, the leaching is prevented. To plasticize a PEO phase, here we suggested modification of OM-AISi with a silane containing a short PEO chain (6-9 units).

2. PEO-modified OM-AISi

As a silane plasticizer, we used [methoxy(polyethylenoxy)propyl]trimethoxysilane (MPEOP) to replace a certain portion of GLYMO in the OM-AISi composition. As can be seen from the data presented in Table 1, a noticeable increase of conductivity occurs already at molar ratio GLYMO:MPEOP = 7:1 (12.5 mol.% MPEOP) for compositions containing both 40 and 55 wt. % of OM-AISi and low molecular weight PEG ($M_n=600$). Further increase of the MPEOP fraction (up to 20 mol.%) does not increase the conductivity, while the SPE film becomes weaker. At the same time, comparison of the temperature dependence of conductivity between the regular SPE and the SPE modified with 12.5 mol. % MPEOP shows that the activation energies (~55 kJ/mol) are similar, so there is no difference in conductivity mechanism.

Comparison of glass transition temperatures for these samples and that of the SPE with a regular hybrid (Table 1) shows that presence of PEO tails attached to Si atoms does provide some decrease in T_g values, but the change of conductivity is not consistent with the glass transition temperature

decrease. Moreover, while for a high molecular weight PEO (100 KDa), T_g changes in a similar fashion, conductivity of these SPE *drops* when the MPEOP modifier is used. Since the SPE films based on 100 KDa PEO are partially crystalline (unlike ones derived from 600 Da PEG),²⁸ we compared their DSC traces (Figure 1) and XRD profiles (Figure 2). Analysis of DSC and XRD data is presented in Tables 1 and 2, respectively. As can be seen from Table 1, the overall crystallinity in the PEO1000-55 samples slightly decreases when 12.5 mol.% GLYMO is replaced with MPEOP and then fully restores when MPEOP fraction is 20 mol.%. One can see a good agreement between DSC and XRD data that supports the credibility of both methods.

A closer look at the DSC melting peaks (Figure 1) shows that the shape of the melting peak changes when MPEOP is introduced. At 20 mol.-% MPEOP (PEO1000-55-MPEOP2), one can see two overlapping peaks, which can be ascribed to two kinds of crystalline species. We believe that along with regular 100 KDa PEO crystallization, the new crystalline phase is formed which includes both PEO and MPEOP PEO tails; thus this phase should form at the OM-AlSi interface.

Analysis of XRD data (Figure 2, Table 2) shows no shift in the positions of the peaks related to two major Bragg planes: d_{032} (cuts across the PEO chain axis) and d_{120} (lies along the PEO chain axis). Since the d_{032} peak cannot be described by a single Gaussian, and probably consists of several peaks, we analyzed only the d_{120} peak, which is well described by single Gaussian. From the data presented in Table 2 one can see a decrease of the d_{120} peak width with an increase of a MPEOP fraction, reflecting some increase in the crystallite size. However, both the combination of a decreased T_g and the slightly increased PEO crystallite size cannot explain the conductivity drop.

In the above discussion we considered only the changes occurring in the organic phase of the hybrid SPE, assuming that the OM-AlSi phase remains unchanged. However, partial replacement of GLYMO with MPEOP might also influence the size and shape of OM-AlSi domains, especially since GLYMO provides both compatibility with PEO and crosslinking due to polymerization of glycidyl groups.²⁸ To estimate the size and shape of OM-AlSi domains, we calcined SPE films at 500 °C for 4 h in nitrogen and 12 h in air, and studied the calcination products. This approach is based on the well-established fact

that the ordered structure of mesoporous oxides prepared by templating over block copolymer templates, well reproduces the structure of the original block copolymer template.³⁶ In our case calcination should provide removal of the organic phase and result in metal oxides (designated AlSi), the structure of which reproduces the structure of OM-AlSi domains.³⁷ Perpetuation of the precursor material structure after calcination was reported in ref. ^{38,39} for hybrid materials containing analogous OM-AlSi, as in this work, and polyisoprene-*block*-poly(ethylene oxide) as a polymeric component. In a preceding paper,⁴⁰ we reported a detailed study of the structure and porosity of the calcined AlSi based on the non-modified SPE. As was shown in ref.⁴⁰, 'PEG+LiTf' domains located in the internal pores of OM-AlSi make no contribution to the Li conductivity process. On the other hand, conductivity was found to depend on the size of OM-AlSi interface, i.e., on the size of OM-AlSi particles formed within the SPE film. This allows us to judge the decrease or increase of the OM-AlSi interface by comparing the sizes of the calcined AlSi particles formed in non-modified and modified OM-AlSi.

Figure 3 presents TEM images of calcined AlSi derived from non-modified PEG6-55 and PEO1000-55 and those of the modified samples with 20 mol.% MPEOP (PEG6-55-MPEOP2 and PEO1000-MPEOP2). For the sample based on low molecular weight PEG (Figure 3 a, b), one can see a noticeable decrease of the AlSi particle size from 30-60 to 15-25 nm, which should be accompanied by an increase of the polymer/OM-AlSi interface area in the non-calcined SPE. The TEM image of the calcined AlSi derived from modified SPE with 12.5 mol.% MPEOP shows a similar pattern. We conjecture that the decrease of the AlSi particle size might be responsible for the conductivity enhancement in the 600 Da PEG series. In contrast, for the 100 KDa PEO series, the AlSi particle size after calcination remains basically unchanged, so the decrease of conductivity *cannot* be ascribed to a significant decrease of the interface area. We believe that formation of a crystalline phase at the OM-AlSi interface (see discussion above) should screen the OM-AlSi surface from participation in Li transport in amorphous PEO regions, and decrease the conductivity. The importance of the interphase region for conductivity will be discussed in more detail in the next section.

3. CN-modified OM-AISi

The addition of cyano groups can serve two purposes. First, being polar, they can increase the dielectric constant of the material and suppress ionic association.⁴¹ Secondly, polyacrylonitrile (PAN) is widely used in gel-like polymer electrolytes since the CN group can coordinate Li and provide transport of Li⁺ ions.^{42,43} As a CN-modifier, we used 2-cyanoethyltrimethoxysilane for partial replacement of GLYMO, varying the CN-modifier fraction from 0 to 50 mol. %. It is worth mentioning that for propionitrile, the structure of which is similar to a CN-modifier tail, the dielectric constant is 29.7 at 20 °C.⁴⁴ This value is much higher than the dielectric constants of OM-AISi (11.0) and PEO (5.0),³⁴ so one might expect better conditions for LiTf dissociation.

To test the role of CN groups, we analyzed the samples by Raman spectroscopy. For triflate anions (CF₃SO₃⁻, or Tf), the symmetric stretching mode of -SO₃ shows the presence of various anionic species, including free or solvent separated Tf (1032 cm⁻¹), contact ion pairs (LiTf, 1042 cm⁻¹), and positively charged aggregates (Li₂Tf⁺, 1052 cm⁻¹).⁴⁵⁻⁴⁸ The contribution of negatively charged triplets (LiTf₂⁻) may also be present in the 1042 cm⁻¹ region. Figure 5 presents Raman spectra for SPEs based on 100 KDa PEO with 55 wt. % OM-AISi. Using PEO with a molecular weight of 100 KDa instead of 600 Da PEG allowed better visualization of changes observed by Raman spectroscopy.⁴⁹ For the sample based on regular OM-AISi (PEO1000-55), one can see two major overlapping bands at 1032 and 1042 cm⁻¹, assigned to free ions and contact ions pairs, respectively. With increase of a CN group fraction, the band characteristic of contact ion pairs decreases, thus suggesting that presence of CN group promotes formation of free ions.

In Figure 4 one can see that the conductivity change with an increase of a CN-modifier fraction depends on the amount of OM-AISi in SPE. In the material containing 70 wt.% OM-AISi (PEG6-70), increase of a CN-modifier fraction first results in doubling the conductivity, then in no change in the range 17.5-37.5 mol.% and finally in a noticeable increase (by a factor of 5) at 50 mol. % of CN-modifier. The SPE films based on 40 % OM-AISi (PEG6-40) also demonstrate three-fold increase in conductivity at the highest CN-modifier content (50 mol. %), but the SPE film becomes too

mechanically weak: OM-AlSi crosslinking due to GLYMO glycidyl groups strongly decreases at overall low (40 wt.%) OM-AlSi content. Similar dependence is observed for the material containing 55 wt.% OM-AlSi (PEG6-55) but the final conductivity gain is weaker.

To probe the influence of the CN-modifier on SPE conductivity, we compared dielectric constants for the materials with different compositions (see Figure 4 and Table 2). In general, the dielectric constants are higher for the materials with lower OM-AlSi fraction that can be explained by a higher overall concentration of LiTf (very polar species) in the material, although the PEO:LiTf molar ratio was kept the same. For all the samples, the higher the dielectric constant (within the experimental error of ~ 0.5), the higher the conductivity, but the increase of conductivity is not linearly consistent with an increase of the CN-modifier fraction. The possible explanation here is that CN groups are not fully exposed to the interface, and their exposure does not necessarily linearly increase with an increase of a CN-modifier fraction.

If CN groups additionally participate in Li ion transfer, one might expect a change of conductivity mechanism that could be detected from variable temperature conductivity measurements. Figure 6 shows variable temperature conductivity dependences of regular SPE with 70 wt.% OM-AlSi (PEG6-70) and of modified materials containing the same amount of OM-AlSi and with 25 (PEG6-70-CN2) and 50 mol.% of CN-modifier (PEG6-70-CN4). The Arrhenius dependence was approximated between 10 and 50°C with calculated activation energies (E_a) about 70 kJ/mol. The similarities of temperature dependences of modified and non-modified samples suggest that CN groups do not directly participate in Li transport, otherwise it should be reflected in the VT conductivity dependencies. For materials containing 40% OM-AlSi, incorporation of CN-modifiers slightly changes the slopes of the VT conductivity dependencies (Fig. 7). The temperature dependencies of conductivity, presented in Figure 7, resemble those of hybrid inorganic-organic polymer electrolytes based on zirconium alkoxide and 400 Da PEG, where polymer chains are short and supposedly chemically attached to zirconium oxide species.³⁰ We fitted these dependencies with two Arrhenius plots. At temperatures above 30 °C, the conductivity is characterized by an activation energy of about 54 kJ/mol, while at lower temperatures

the activation energy reaches 70-73 kJ/mol depending on a CN-modifier fraction. Here, the VT conductivity dependences of the CN-modified samples slightly differ from that of regular PEO6-40, but still the difference is negligible.

The data of Table 3, show that for SPE based on 40 and 55%, there is no clear dependence of T_g on the OM-AlSi fraction, while for SPE based on 70% CN-modifier, T_g values are noticeably higher for CN-modified SPE. Evidently, there is no correlation between T_g and conductivity changes.

To understand the influence of CN-modifier on OM-AlSi morphology, we carried out a TEM study of calcined AlSi as described above for the MPEOP-modifier. Figure 8 shows TEM images of the calcined AlSi derived from PEG6-70, PEG6-70-CN1, and PEG6-70-CN4, as these two modified samples show the largest steps in conductivity increase for 70% OM-AlSi series. One can see that the size of AlSi particles changes as CN-modifier amount increases. In AlSi derived from regular PEG6-70, the smallest particles measure 40-60 nm, yet, their fraction is low and larger particles prevail. Incorporation of 17.5% CN-modifier results in a higher fraction of particles measuring 25-60 nm. Increase of CN-modifier fraction to 50% leads to a high fraction of AlSi particles measuring 32-45 nm with fewer larger particles. Thus, the trend is a decrease of the AlSi particle size, i.e., an increase of the interfacial area, with an increase of the CN-modifier fraction. For materials based on 40% OM-AlSi, this trend is even more prominent. In Figure 9 one can see that for 17.5% of CN-modifier, AlSi particles are in the range 45-75 nm. For 25% of CN-modifier, the majority of the particles are in the range of 33-65 nm. Incorporation of 37.5 and 50% of CN-modifier leads to mean particle sizes of 30 and 13 nm, respectively. Thus, increase of the CN-modifier fraction results in smaller OM-AlSi domains and higher interfacial area. If it is accompanied with higher exposure of the CN groups at the interface, it can lead to a higher dielectric constant. If the increase in the amount of CN groups at the interface does not coincide with the increase of the interfacial area, dielectric constant does not increase, while conductivity still might increase.

The importance of the interface for conductivity of hybrid materials with inorganic fillers was explored in a number of publications.^{7-10,50} It is assumed that an ion-conducting pathway exists at the

interphase between the fillers and the polymer even prior to percolation.¹⁰ This interphase is formed due to interaction of Li ions at the filler interface supposedly with Lewis acid groups. The larger the interface, the more groups can be exposed to Li ions, and the higher the conductivity. In the SPE reported here, the Lewis acid sites are formed by tetrahedral aluminum (AlO_4^-).²⁸ As detected by ^{27}Al MAS NMR (Figure 10), the amount of tetrahedral aluminum species increases when CN-modifier is first introduced and then only slightly increases with an increase of the CN-modifier fraction. Thus, exposure of the Lewis acid sites to the OM-AlSi interface cannot increase dramatically without interface increase. At the same time, the larger the amount of Lewis acid sites contacting with PEO+LiTf, the greater their influence on Li transport. The increase of the dielectric constant of the interphase layer due to CN groups, combined with the increase of the interface area, should lead to the increase of conductivity due to enhancement of Li ion-conducting pathway. When the OM-AlSi/PEO+LiTf interphase (in the case of 100 KDa PEO series with MPEOP modifier) contains a crystalline PEO phase, the ion-conducting pathway is impeded, decreasing the conductivity.

Conclusions

We studied modification of a hybrid SPE, based on OM-AlSi and PEO+Li triflate phase, with organically modified silanes containing a short PEO tail (MPEOP-modifier) or CN group (CN-modifier). This modification can result in significant enhancement of conductivity, if incorporation of a silane-modifier increases the interphase between OM-AlSi and PEO+LiTf phase by decreasing the OM-AlSi domain size. Presence of CN groups at the OM-AlSi/PEO+LiTf interface increases the dielectric constant of the interphase layer, thus suppressing the LiTf association and increasing the conductivity. At the same time, variable temperature conductivity dependences show no indication of the conductivity mechanism change in the modified SPE reported here.

ACKNOWLEDGMENT. The authors thank NASA for grant NAG3-2588 for financial support of this project.

References

- (1) Scrosati, B. *Nature* **1995**, 373(6515), 557.
- (2) Nookala, M.; Kumar, B.; Rodrigues, S. *J. Power Sourc.* **2002**, 111, 165.
- (3) Wang, C.; Xia, Y.; Koumoto, K.; Sakai, T. *J. Electrochem. Soc* **2002**, 149, A967.
- (4) Persi, L.; Croce, F.; Scrosati, B.; Plichta, E.; Hendrickson, M. A. *J. Electrochem. Soc* **2002**, 149, A212.
- (5) Li, Q.; Imanishi, N.; Takeda, Y.; Hirano, A.; Yamamoto, O. *Ionics* **2002**, 8, 79.
- (6) Digar, M.; Hung, S.-L.; Wen, T.-C. *J. Appl. Polym. Sci.* **2001**, 80, 1319.
- (7) Wieczorek, W.; Lipka, P.; Zukowska, G.; Wycislik, H. *J. Phys. Chem. B* **1998**, 102, 6968.
- (8) Best, A. S.; Adebahr, J.; Jacobsson, P.; MacFarlane, D. R.; Forsyth, M. *Macromolecules* **2001**, 34, 4549.
- (9) Marcinek, M.; Bac, A.; Lipka, P.; Zalewska, A.; Zukowska, G.; Borkowska, R.; Wieczorek, W. *J. Phys. Chem. B* **2000**, 104, 11088.
- (10) Adebahr, J.; Best, A. S.; Byrne, N.; Jacobsson, P.; MacFarlane, D. R.; Forsyth, M. *Phys.Chem.Chem.Phys.* **2003**, 5, 720.
- (11) Cheung, I. W.; Chin, K. B.; Greene, E. R.; Smart, M. C.; Abbrent, S.; Greenbaum, S. G.; Prakash, G. K. S.; Surampudi, S. *Electrochim. Acta* **2003**, 48, 2149.
- (12) Meyer, W. H. *Adv. Mater.* **1998**, 10, 439.
- (13) Sadoway, D. R.; Huang, B. Y.; Trapa, P. E.; Soo, P. P.; Bannerjee, P.; Mayes, A. M. *J. Power Sourc.* **2001**, 97-98, 621.
- (14) Soo, P. P.; Huang, B. Y.; Jang, Y. I.; Chiang, Y. M.; Sadoway, D. R.; Mayes, A. M. *J. Electrochem. Soc* **1999**, 146, 32.
- (15) Bloise, A. C.; Tambelli, C. C.; Franco, R. W. A.; Donoso, J. P.; Magon, C. J.; Souza, M. F.; Rosario, A. V.; Pereira, E. C. *Electrochim. Acta* **2001**, 46, 1571.
- (16) Croce, F.; Persi, L.; Scrosati, B.; Serraino-Fiory, F.; Plichta, E.; Hendrickson, M. A. *Electrochim. Acta* **2001**, 46, 2457.

- (17) Scrosati, B.; Croce, F.; Panero, S. *J. Power Sourc.* **2001**, *100*, 93.
- (18) Weston, J. E.; Steele, B. C. H. *Solid State Ionics* **1982**, *7*, 75.
- (19) Croce, F.; Appetecchi, G. B.; Persi, L.; Scrosati, B. *Nature* **1998**, *394(6692)*, 456.
- (20) Krawiec, W.; Scanlon, L. G. J.; Fellner, J. P.; Vaia, R. A.; Vasudevan, S.; Giannelis, E. P. *J. Power Sourc.* **1995**, *54*, 310.
- (21) Vaia, R. A.; Vasudevan, S.; Krawiec, W.; Scanlon, L. G.; Giannelis, E. P. *Adv. Mater.* **1995**, *7*, 154.
- (22) Giannelis, E. P. *Adv. Mater.* **1996**, *8*, 29.
- (23) Lemmon, J. P.; Wu, J.; Oriakhi, C.; Lerner, M. M. *Electrochim. Acta* **1995**, *40*, 2245.
- (24) Hutchison, J. C.; Bissessur, R.; Shriver, D. F. *Chem. Mater.* **1996**, *8*, 1597.
- (25) Tambelli, C. C.; Bloise, A. C.; Rosario, A. V.; Pereira, E. C.; Magon, C. J.; Donoso, J. P. *Electrochim. Acta* **2002**, *47*, 1677.
- (26) Johansson, P.; Ratner, M. A.; Shriver, D. F. *J. Phys. Chem.* **2001**, *105*, 9016.
- (27) Popall, M.; Andrei, M.; Kappel, J.; Kron, J.; Olma, K.; Olsowski, B. *Electrochim. Acta* **1998**, *43*, 1155.
- (28) Bronstein, L. M.; Joo, C.; Karlinsey, R.; Ryder, A.; Zwanziger, J. W. *Chem. Mater.* **2001**, *13*, 3678.
- (29) Jiang, S.; Yu, D.; Ji, X.; An, L.; Jiang, B. *Polymer* **2000**, *41*, 2041.
- (30) Di Noto, V.; Zago, V.; Biscazzo, S.; Vittadello, M. *Electrochim. Acta* **2003**, *48*, 541.
- (31) Ulrich, R.; Zwanziger, J. W.; De Paul, S. M.; Richert, R.; Wiesner, U.; Spiess, H. W. *Polym. Mat. Sci. Eng.* **1999**, *80*, 610.
- (32) Ulrich, R.; Zwanziger, J. W.; De Paul, S. M.; Reiche, A.; Leuninger, H.; Spies, H. W.; Wiesner, U. *Adv. Mater.* **2002**, *14*, 1134.
- (33) Templin, M.; Wiesner, U.; Spies, H. W. *Adv. Mater.* **1997**, *9*, 814.
- (34) McCrum, N. G.; Read, B. E.; Williams, G. *Anelastic and Dielectric Effects in Polymeric Solids*; Dover: New York, 1967.

- (35) Takahashi, Y.; Tadokoro, H. *Macromolecules* **1973**, *6*, 672.
- (36) Göltner, C. G.; Henke, S.; Weissenberger, M. C.; Antonietti, M. *Angew. Chem. Intern. Ed.* **1998**, *37*, 613.
- (37) Goltner, C. G.; Henke, S.; Weissenberger, M. C.; Antonietti, M. *Angew. Chem. Intern. Ed.* **1998**, *37*, 613.
- (38) Finnefrock, A. C.; Ulrich, R.; Du Chesne, A.; Honeker, C. C.; Schumacher, K.; Unger, K. K.; Gruner, S. M.; Wiesner, U. *Angew. Chem. Intern. Ed.* **2001**, *40*, 1208.
- (39) Simon, P. F. W.; Ulrich, R.; Spies, H. W.; Wiesner, U. *Chem. Mater.* **2002**, *13*, 3464.
- (40) Bronstein, L. M.; Ashcraft, E.; DeSanto, P., Jr.; Karlinsey, R. L.; Zwanziger, J. W. *J. Phys. Chem. B* **2003**, *submitted*.
- (41) Bishop, A. G.; MacFarlane, D. R.; McNaughton, D.; Forsyth, M. *J. Phys. Chem.* **1996**, *1000*, 2237.
- (42) Watanabe, M.; Kanba, M.; Nagaoka, K.; Shinohara, I. *J. Appl. Polym. Sci.* **1982**, *27*, 4191.
- (43) Akashi, H.; Shibuya, M.; Orui, K.; Shibamoto, G.; Sekai, K. *J. Power Sourc.* **2002**, *112*, 577.
- (44) Dannhauser, W.; Flueckinger, A. F. *J. Phys. Chem.* **1964**, *68*, 1814.
- (45) Peterson, G.; Jacobsson, P.; Torell, L. M. *Electrochim. Acta* **1992**, *37*, 1495.
- (46) Ferry, A. *J. Phys. Chem. B* **1996**, *101*, 150.
- (47) Frech, R.; Huang, W. *Macromolecules* **1995**, *28*, 1246.
- (48) Frech, R.; Chintapalli, S.; Bruce, P. G.; Vincent, C. A. *Chem. Commun.* **1997**, 157.
- (49) Joo, C. G.; Bronstein, L. M.; Karlinsey, R. L.; Zwanziger, J. W. *Solid State Nucl. Magn. Reson.* **2002**, *22*, 235.
- (50) Forsyth, M.; MacFarlane, D. R.; Best, A.; Adebahr, J.; Jacobsson, P.; Hill, A. J. *Solid State Ionics* **2002**, *14*, 203.

Table 1. Room temperature conductivities and structural characteristics of SPE with a MPEOP modifier

sample notation	GLYMO:MPEOP (mol)	T _g , °C	ΔH, J/g	crystallinity, %*	ε _r	Conductivity, S/cm
PEG6-40	-	-54	-	-	29.1	2.95 10 ⁻⁵
PEG6-40-MPEOP1	1:7	-56	-	-	23.9	1.05 10 ⁻⁴
PEG6-55	-	-52	-	-	17.2	1.35 10 ⁻⁵
PEG6-55-MPEOP1	1:7	-55	-	-	20.3	5.73 10 ⁻⁵
PEG6-55-MPEOP2	1:4	-57	-	-	18.1	5.18 10 ⁻⁵
PEO1000-55	-	-42	25.02	~60	16	3.79 10 ⁻⁵
PEO1000-55-MPEOP1	1:7	-49	23.43	~56	12.2	6.82 10 ⁻⁶
PEO1000-55-MPEOP2	1:4	-47	25.87	~60	12.0	7.61 10 ⁻⁶

*obtained from XRD data

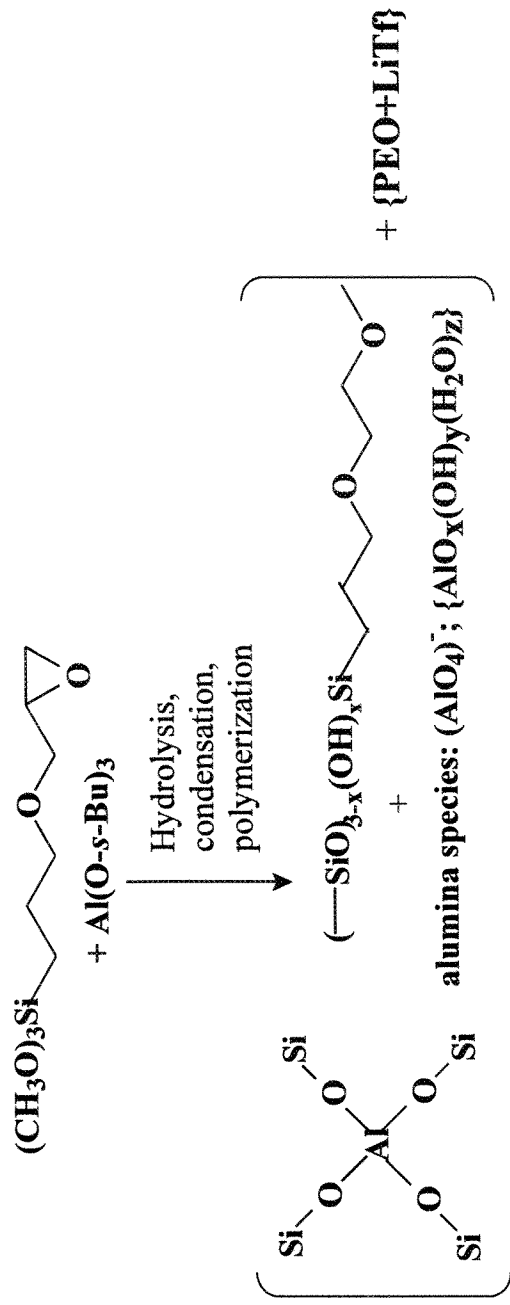
Table 2. Analysis of d_{120} in XRD data of SPE samples based on 100 KDa PEO.

sample notation	center of gravity ^{a)} , \AA^{-1}	FWHM ^{b)} , \AA^{-1}	crystallite size, nm
PEO1000-55	1.365	0.039	32 ± 3
PEO1000-55-MPEOP1	1.358	0.034	37 ± 5
PEO1000-55-MPEOP2	1.360	0.029	44 ± 6

^{a)}Error is 0.002\AA^{-1} , ^{b)} Full Width at Half Maximum (FWHM) error is 0.004\AA^{-1} .

Table 3. Characteristics of hybrid SPE modified with CN-modifier

sample notation	CN-modifier, mol. %	T _g , °C	dielectric constant	conductivity, S/cm
PEG6-40	0	-54	29.1	2.88 10 ⁻⁵
PEG6-40-CN1	17.5	-56	35.9	3.94 10 ⁻⁵
PEG6-40-CN2	25.0	-55	51.5	6.21 10 ⁻⁵
PEG6-40-CN3	37.5	-57	56.8	7.75 10 ⁻⁵
PEG6-40-CN4	50.0	-56	69.0	1.06 10 ⁻⁴
PEG6-55	0	-54	17.2	1.58 10 ⁻⁵
PEG6-55-CN1	17.5	-57	11.2	1.24 10 ⁻⁵
PEG6-55-CN2	25.0	-56	15.0	1.72 10 ⁻⁵
PEG6-55-CN3	37.5	-54	15.0	1.99 10 ⁻⁵
PEG6-55-CN4	50.0	-52	18.9	3.83 10 ⁻⁵
PEG6-70	0	-42	13.6	1.71 10 ⁻⁶
PEG6-70-CN1	17.5	-48	13.4	3.33 10 ⁻⁶
PEG6-70-CN2	25.0	-47	11.6	3.00 10 ⁻⁶
PEG6-70-CN3	37.5	-56	12.5	3.54 10 ⁻⁶
PEG6-70-CN4	50.0	-50	15.1	9.29 10 ⁻⁶



Scheme 1. Depiction of the SPE composition based on organically modified aluminosilicate (OM-AISi) and PEO with Li triflate.

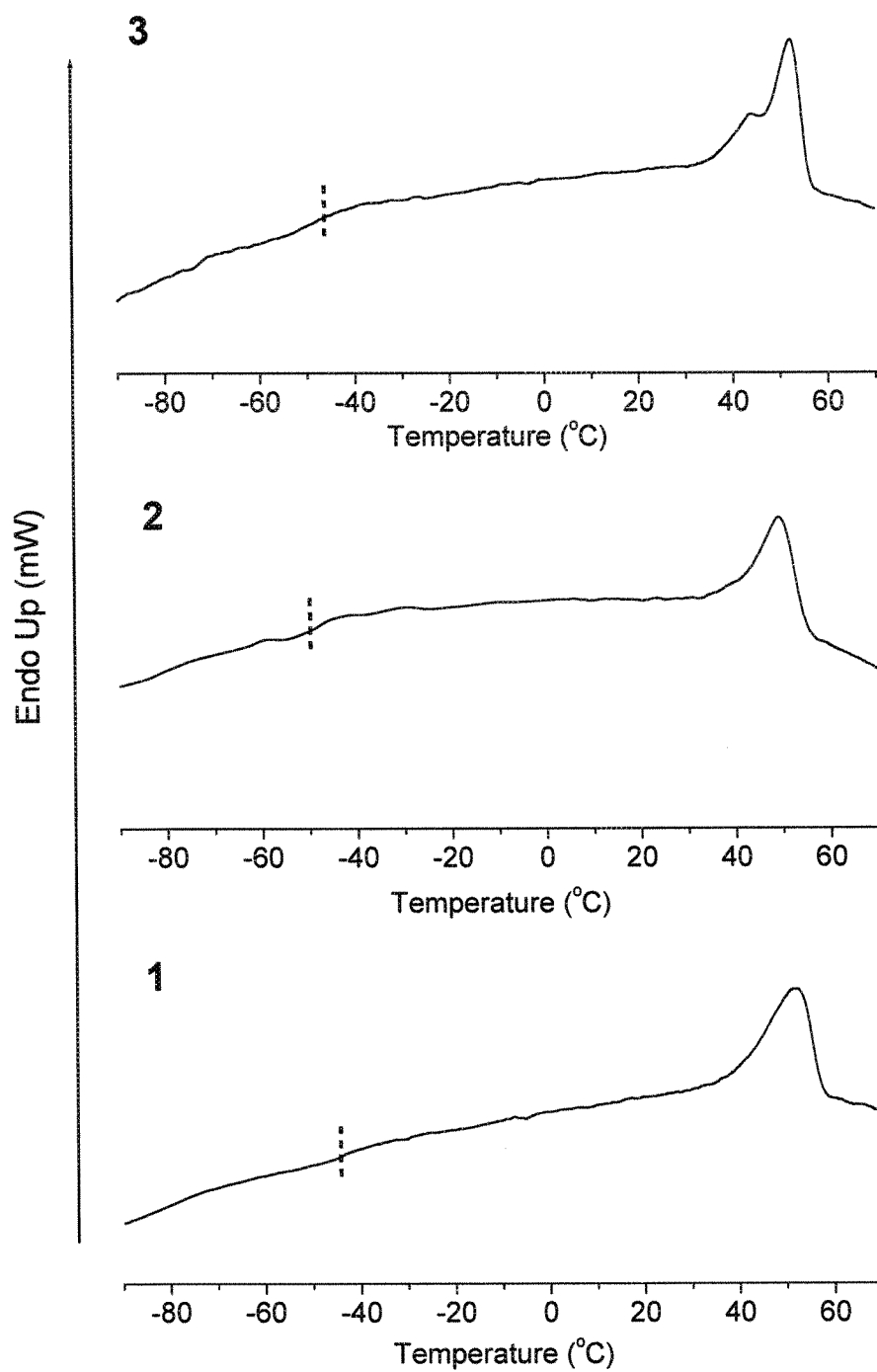


Figure 1. DCS traces of PEO1000-55 (1), PEO1000-55-MPEOP1 (2), and PEO1000-55-MPEOP2 (3). Glass transitions are indicated with a dashed line. Deconvolution of melting is shown in the inset under the melting transition.

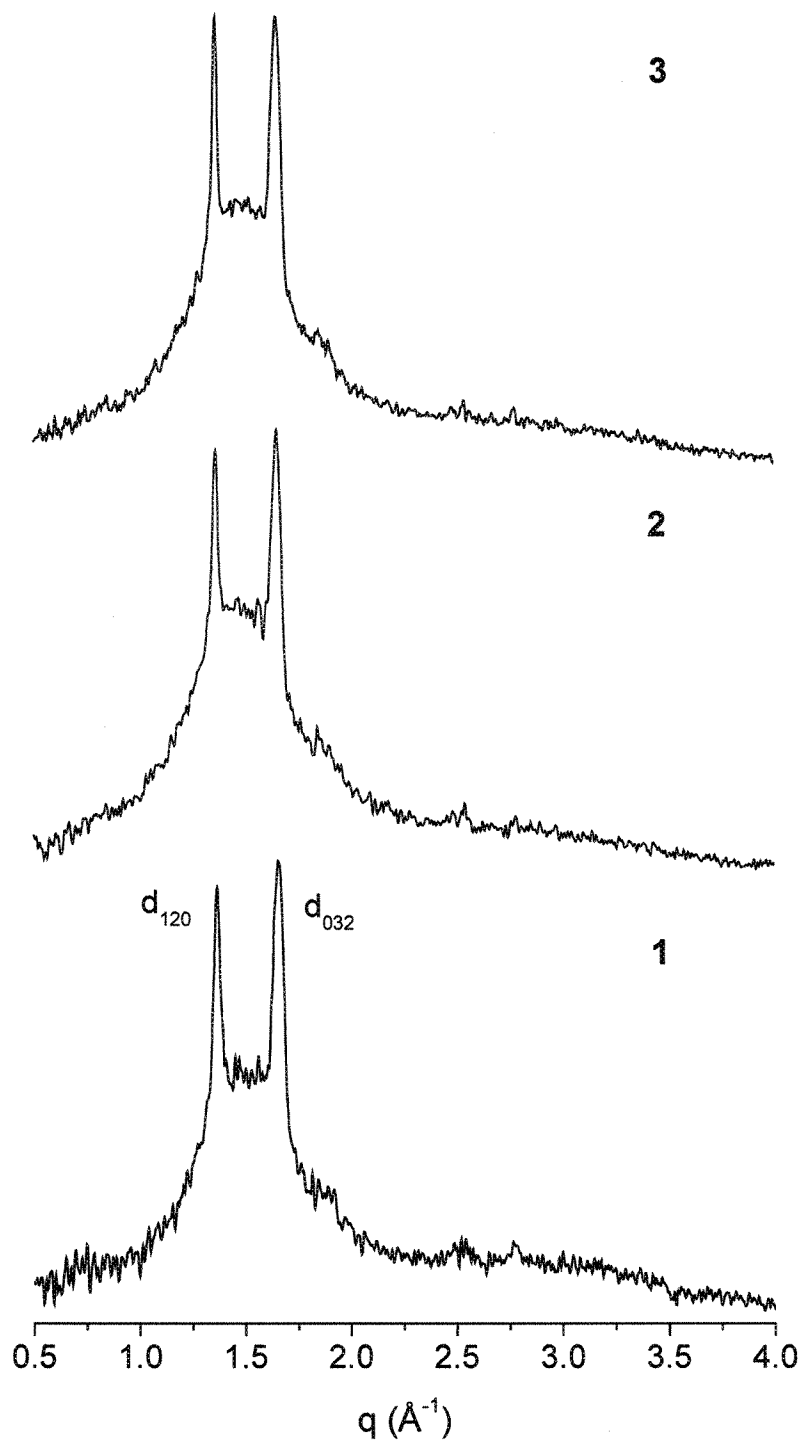


Figure 2. XRD profiles of PEO1000-55 (1), PEO1000-55-MPEOP1 (2), and PEO1000-55-MPEOP2 (3). The Bragg assignments are shown for the two principle crystalline features.

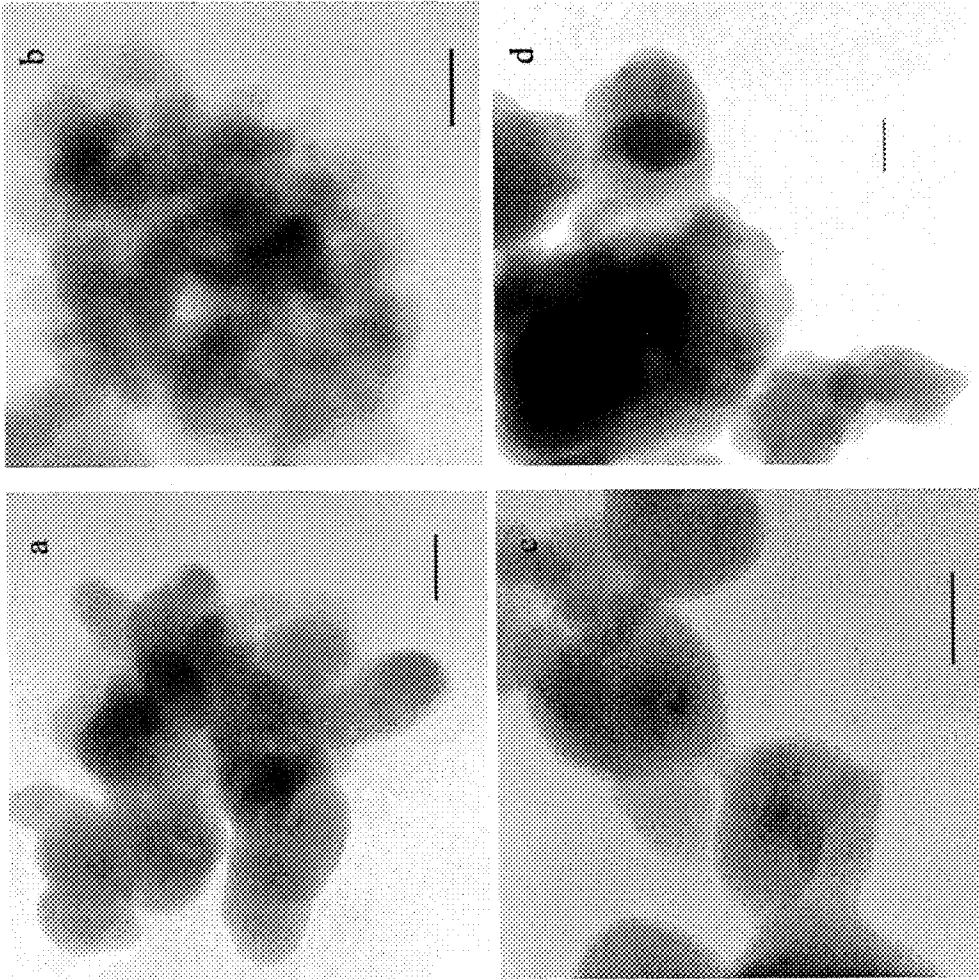


Figure 3. TEM images of calcined AISi derived from PEG6-55 (a), PEG6-55-GEL2 (b), PEO1000-55 (c), and PEO1000-55GEL2 (d). Scale bar is 50 nm.

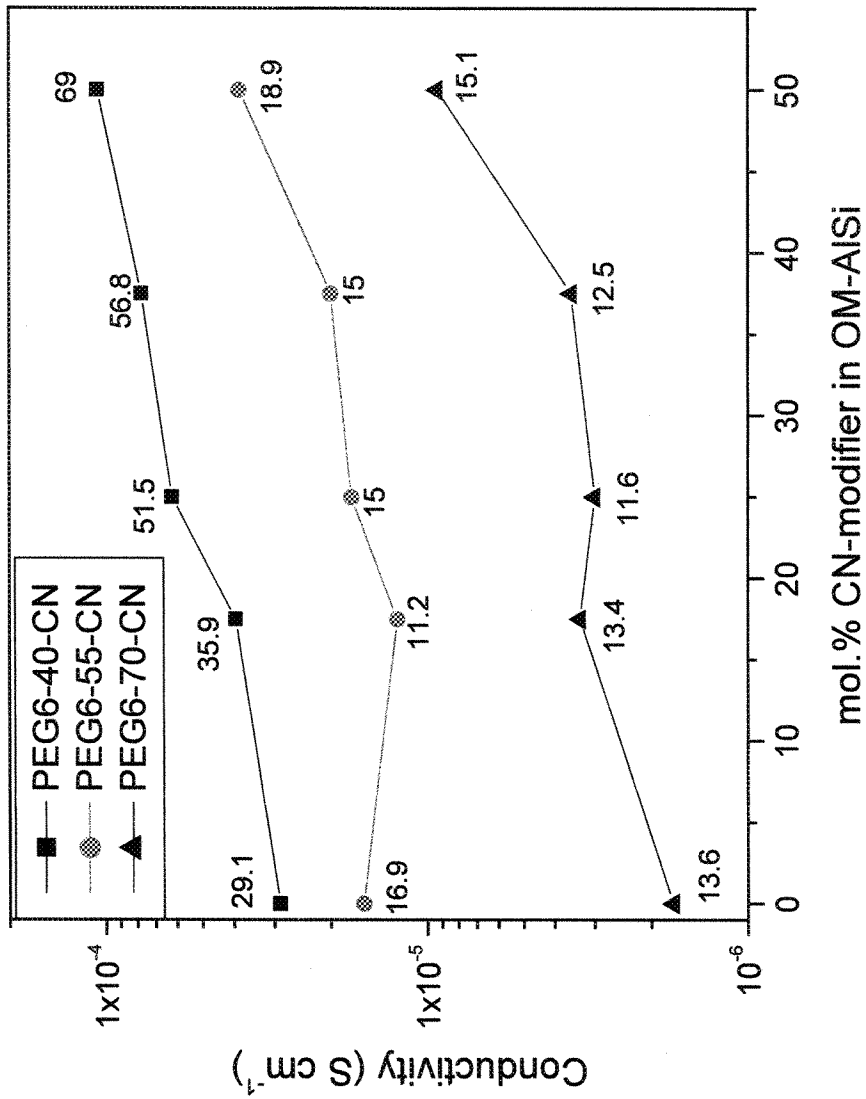


Figure 4. Dependences of conductivity on a CN-modifier fraction for different hybrid SPE. Numbers at data points stand for dielectric constant.

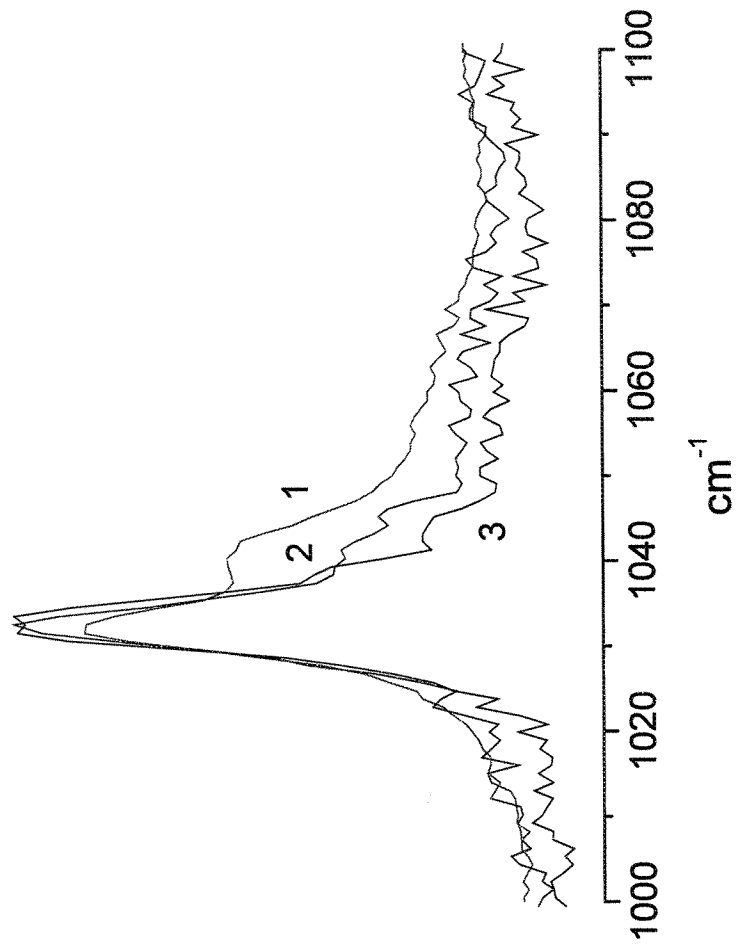


Figure 5. Raman spectra in the symmetric stretching mode of -SO_3 for PEO1000-55 (1), PEO1000-55-CN1 (2) and PEO1000-55-CN2 (3).

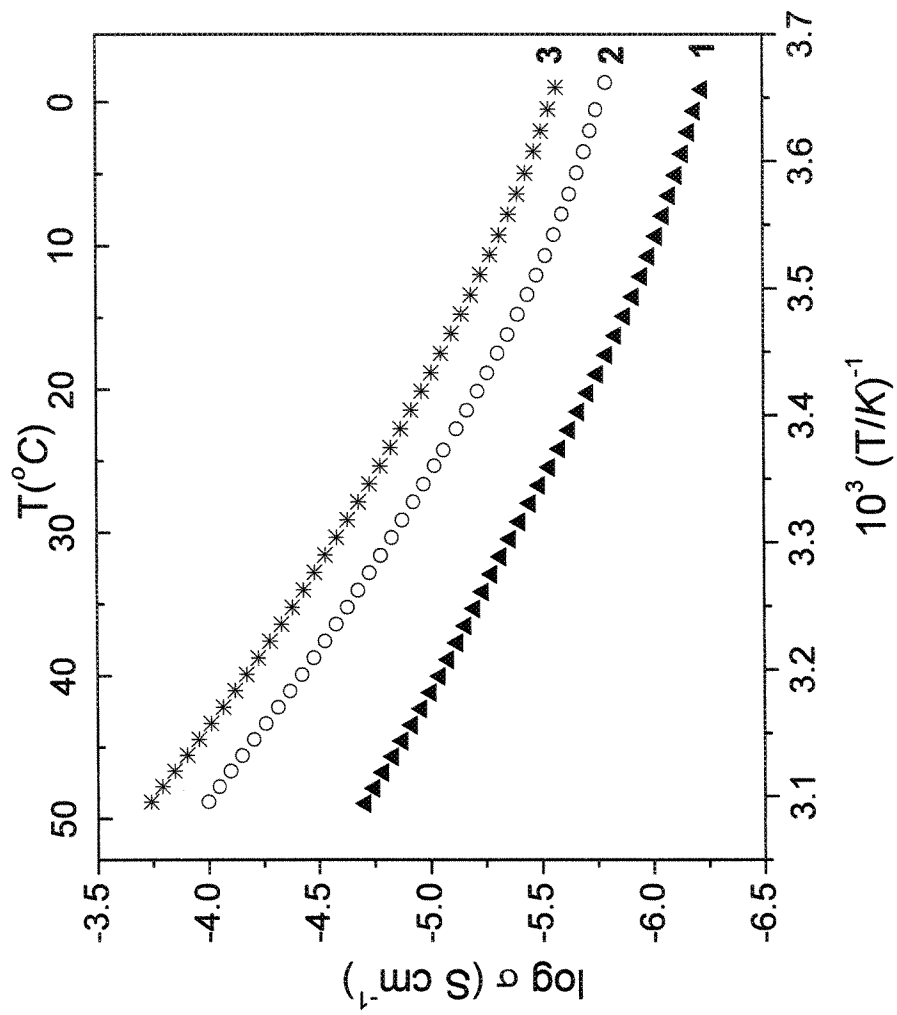


Figure 6. Temperature dependences of conductivities for PEG6-70 (1), PEG6-70-CN2 (2), and PEG6-70-CN4 (3).

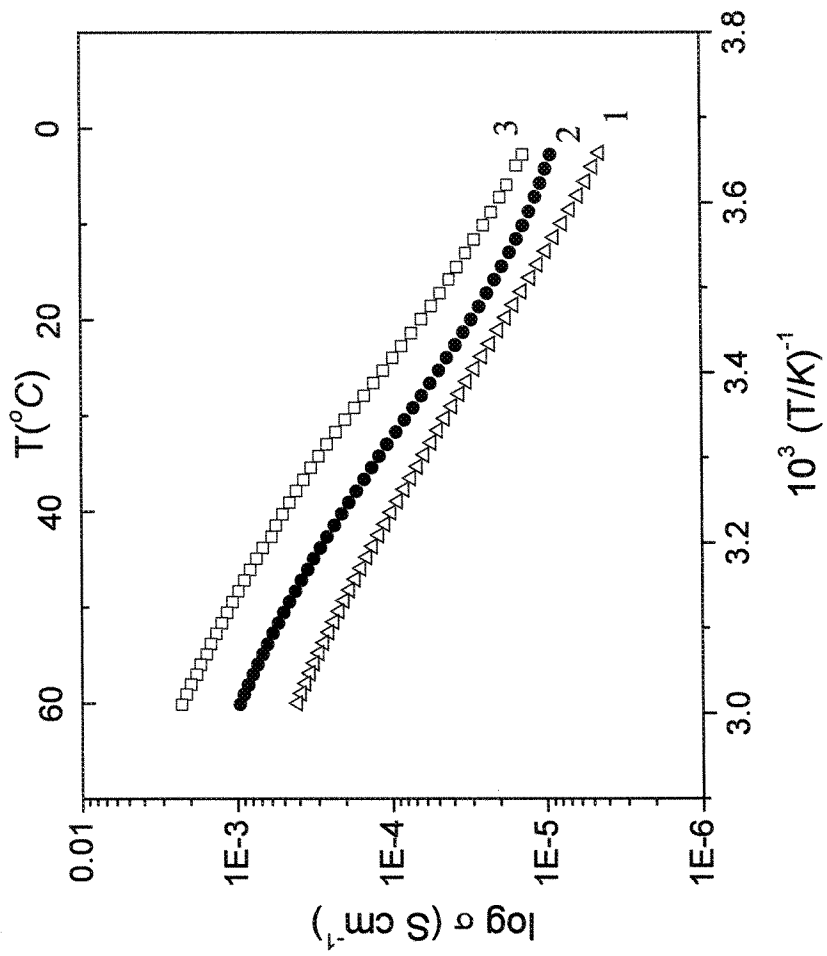


Figure 7. Temperature dependences of conductivities for PEG6-40 (1), PEG6-40-CN1 (2), and PEG6-40-CN3 (3).

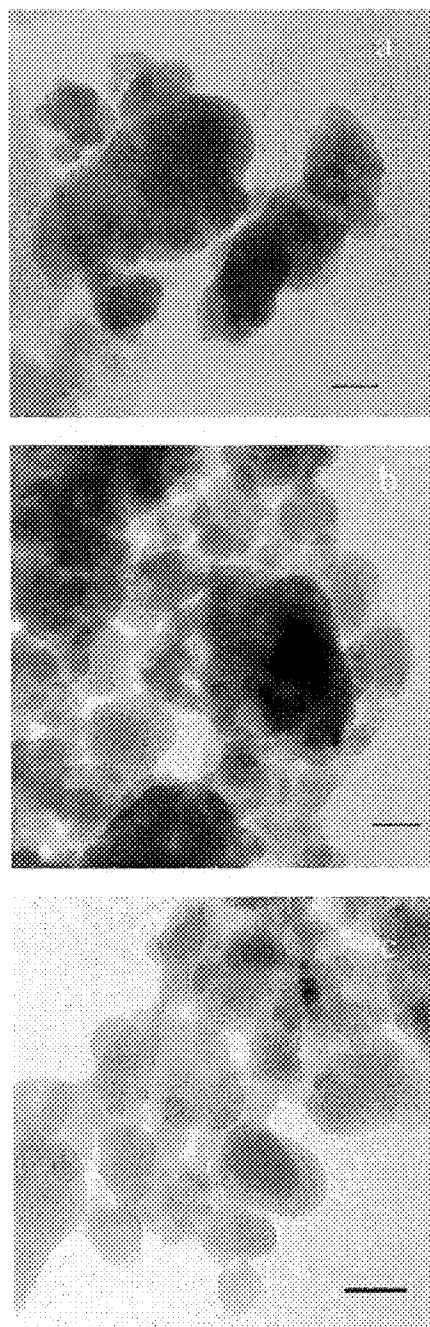


Figure 8. TEM images of the calcined AlSi derived from PEG6-70 (a), PEG6-70-CN1 (b), and PEG6-70-CN4. Scale bar is 50 nm.

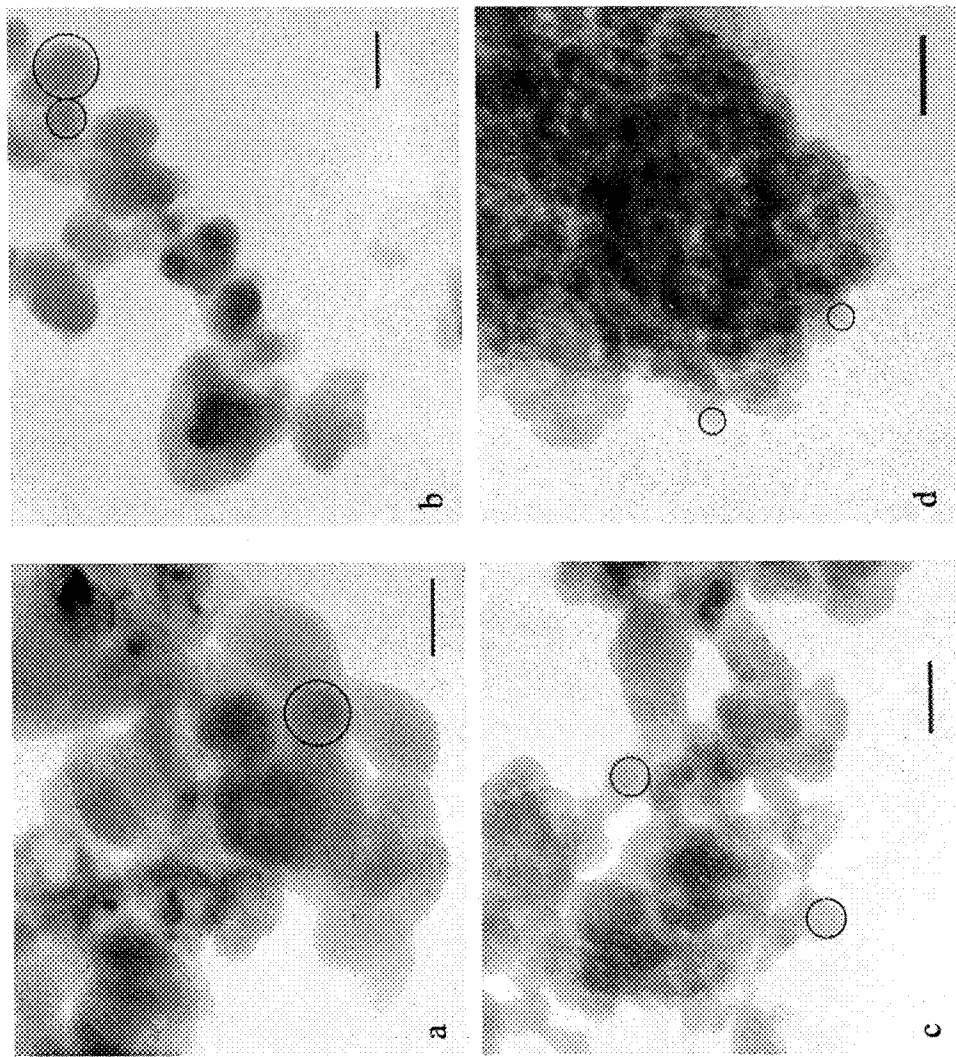


Figure 9. TEM images of the calcined AISi derived from PEG6-40-CN1 (a), PEG6-40-CN2 (b), PEG6-40-CN3 (c), and PEO4-70-CN4 (d). Scale bar is 50 nm. Circles show the individual particle profiles.

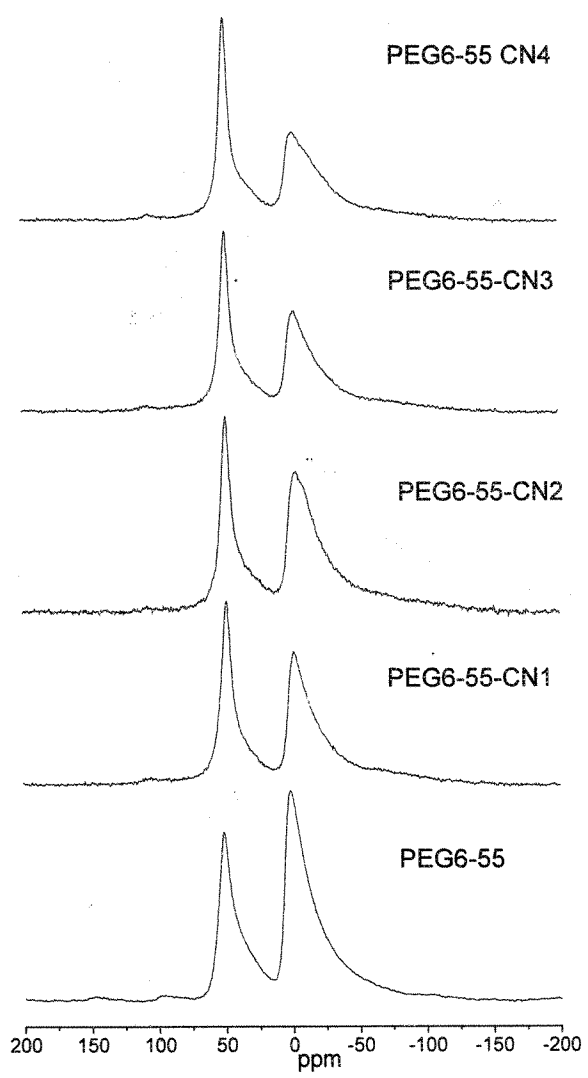


Figure 10. ^{27}Al MAS NMR spectra of non-modified SPE and SPE modified with CN-modifier.